Journal of
www. biophotonics-journal.org

BIOPHOTONICS

WILEY-VCH

J. Biophotonics 9, No. 1–2, 38–43 (2016) / **DOI** 10.1002/jbio.201500192

Journal of BIOPHOTONICS

LETTER

Transmission in near-infrared optical windows for deep brain imaging

Lingyan Shi[*, 1, 2], *Laura A. Sordillo*[1], *Adrián Rodríguez-Contreras*[1, 2], *and Robert Alfano*[1]

[1] Institute for Ultrafast Spectroscopy and Lasers, Department of Physics, the City College of the City University of New York, 160 Convent Avenue, New York, NY 10031, USA
[2] Department of Biology, the City College of the City University of New York, 160 Convent Avenue, New York, NY 10031, USA

Received 8 July 2015, revised 14 October 2015, accepted 21 October 2015
Published online 11 November 2015

Key words: near-infrared, deep brain imaging, transmittance, golden optical tissue window, total attenuation length

Near-infrared (NIR) radiation has been employed using one- and two-photon excitation of fluorescence imaging at wavelengths 650–950 nm (optical window I) for deep brain imaging; however, longer wavelengths in NIR have been overlooked due to a lack of suitable NIR-low band gap semiconductor imaging detectors and/or femtosecond laser sources. This research introduces three new optical windows in NIR and demonstrates their potential for deep brain tissue imaging. The transmittances are measured in rat brain tissue in the second (II, 1,100–1,350 nm), third (III, 1,600–1,870 nm), and fourth (IV, centered at 2,200 nm) NIR optical tissue windows. The relationship between transmission and tissue thickness is measured and compared with the theory. Due to a reduction in scattering and minimal absorption, window III is shown to be the best for deep brain imaging, and windows II and IV show similar but better potential for deep imaging than window I.

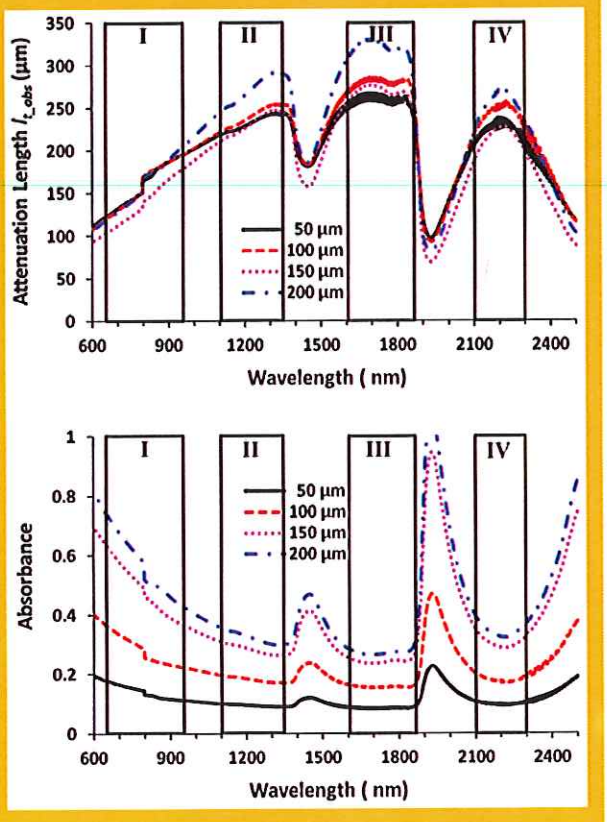

* Corresponding author: e-mail: lshl365@gmail.com

1. Introduction

Brain tissue is a unique tissue compared to other tissues in the body. It contains twice as much lipid and less than half of the protein found in muscle tissue [1]. One of the major thrusts in neuroscience is to image deep inside the brain. The current technique of magnetic resonance imaging (MRI) provides images with poor spatial resolution at millimeter scale. Optical imaging is still the only method to study neural tissues with micrometer or sub-micrometer resolution. When a light pulse propagates in tissue media it divides into separate components, a ballistic, a snake and diffusive components [2, 3]. Light possesses several salient properties including wavelength, polarization, coherence and the shortest pulses that can be used to probe and better understand tissue structure and functions [3]. However, light application is also limited due to scattering and absorption: scattering blurs images while absorption reduces the number of available photons.

Compared with the application of light at shorter wavelengths in the visible range, near infrared (NIR) spectral zone from 650–950 nm (defined as tissue optical window I, also known as the therapeutic window) has the advantages of reduced absorption and scattering, deeper penetration, and most of all, the availability of silicon-based photo detectors. The NIR optical window I has been conventionally used for imaging studies [4]. Application of two-photon microscopy can achieve deep imaging by using the ballistic component of NIR light for excitation in the tissue optical window I. To further increase the imaging depth, one solution is to excite fluorescent agents to their second singlet (S_2) state, where both the excitation and emission wavelengths fall within the optical window, which would greatly enhance the imaging depth [5]. The difficulty of the S_2 pumping technique lies in the lack of proper quantum dots or dyes that can be used. An alternate solution is to apply longer NIR wavelengths for tissue imaging, such that the scattering and absorption are further decreased due to theories of Rayleigh scattering and Mie scattering. The scattering coefficient decreases with increasing wavelength into NIR. Imaging using these longer wavelengths has been overlooked either due to lack of suitable NIR complementary metal-oxide semiconductor (CMOS) imaging detectors and/or lack of suitable femtosecond laser sources.

Recently, using indium gallium arsenide-(InGaAs) or indium antimonide-(InSb-)based detectors and a femtosecond excitation source of IMRA fiber laser (excitation wavelength 1680 nm, power >200 mW, pulse width 100 fs, and 50 MHz repetition rate), Sordillo et al. [6] reported imaging of tissues in the NIR regions, namely window II (1,100–1,350 nm), window III (1,600–1,870 nm), and window IV (centered at 2,200 nm) using lamp and supercontinuum laser source. Their study demonstrates the potential for greater imaging depth in these optical windows and their complementary wavelengths. The present study further investigates the optimal wavelength band and optical properties of brain tissue in NIR, including the total attenuation coefficient (μ_t), absorption coefficient (μ_a), reduced scattering coefficient (μ_s') and the scattering anisotropy coefficient (g) in these optical windows. The transmission at these three windows in rat brain tissues were measured and compared with a theoretical model incorporating ballistic and diffusive components. The purpose of the study was to determine an optimal optical window in NIR from 650 nm to 2500 nm by giving the total attenuation length (l_t) for ballistic imaging to reduce scattering with optimal absorption and further reduce noise for deep brain tissue imaging.

2. Materials and methods

2.1 Experiments

Experimental procedures were reviewed and approved by the Institutional Animal Care and Use Committee of the City College of New York. Timed-pregnant first time Wistar rats were obtained at E15 (Charles River Laboratories) and housed at the City College Animal Facility under conditions described previously [7].

A 9-day old rat was injected with a mixture of ketamine (41.7 mg/kg) and xylazine (2.5 mg/kg body). Depth of anesthesia was checked by toe pinch reflex of upper and lower extremities. After the rat was completely anesthetized, it was perfused intracardially with 4% formaldehyde in 0.1 M phosphate buffer (PB) at cardiac output rate using a syringe pump [8, 9]. The brain was dissected and postfixed overnight and subsequently immersed in 30% sucrose in 0.1 M PB for up to 48 hrs prior to slicing. The brain was sliced at thicknesses of 50 μm, 100 μm, 150 μm and 200 μm by using a freezing stage microtome (American Optical, Buffalo, NY).

A Cary 500 scan UV/VIS/NIR spectrophotometer was used for measuring the transmittance from the spectrum 600–2500 nm with a 1 nm bandwidth. The brain tissue was placed on a thin quartz slide that was stabilized on a sample holder. For each brain slice, the light beam would pass through the grey matter and the intensity of light reaching the detector was measured.

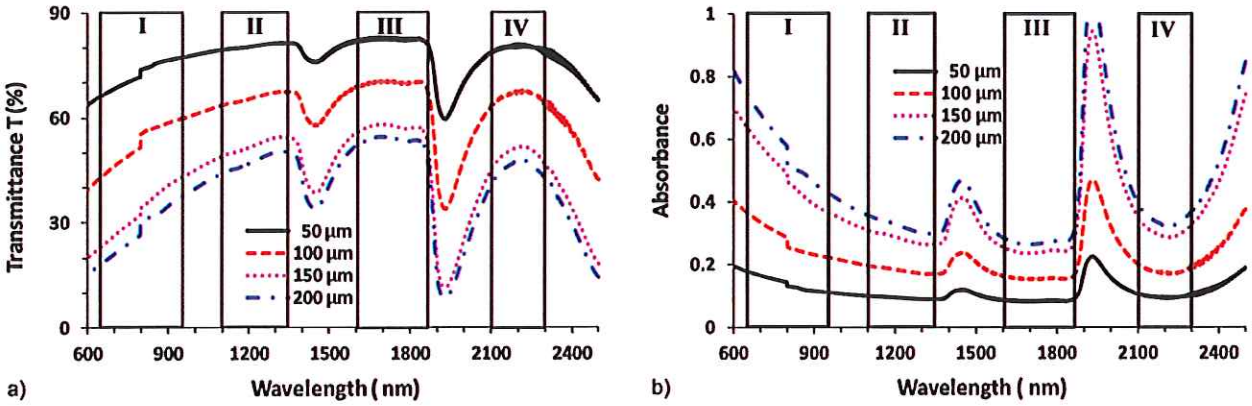

Figure 1 Transmittance T (%) (a) and absorbance (b) in optical tissue windows I, II, III and IV. Brain tissue thicknesses were 50, 100, 150, and 200 µm respectively.

2.2 *Theory*

The salient parameters in optical imaging methods depend on some key factors, including the total attenuation length (l_t), the mean free scattering length (l_s), the absorption length (l_a), the transport length (l_{tr}), and scattering anisotropy coefficient (g). Correspondingly, these lengths are related to attenuation coefficient μ_t (= $1/l_t$), scattering coefficient μ_s (= $1/l_s$), absorption coefficient μ_a (= $1/l_a$), and reduced scattering coefficient μ_s' (= $1/l_{tr}$), with $\mu_t = \mu_s + \mu_a$, and $\mu_s' = \mu_s(1 - g)$, where g is the anisotropy angular factor, which equals 0.7 to 0.98 for tissue, and approximately 1 and 0 for large particles and small particles, respectively.

The ballistic photons in scattering media are governed by the Beer-Lambert law:

$$T = \frac{I}{I_0} = \exp(-\mu_t z) = \exp\left(-\frac{z}{l_t}\right), \quad (1)$$

where I is the intensity of transmitted light, I_0 is the intensity of incident light, z is the light path (or, tissue thickness). The transmittance measured in experiments by two-photon microscopy can be used to calculate the l_t by using Eq. (1).

3. Results and discussion

Figure 1(a) shows the transmittance T (%) measured for the brain tissues in each optical window, and Table 1 summarizes the peak transmittances of brain tissues in these windows. Maximum peak transmittances are all located in window III for tissues with thickness 50, 100, 150, and 200 µm. Peak transmittances in windows II and IV are close to each other and are much higher than those in window I, showing their better potential for deep imaging than window I. Figure 1(b) shows the absorbance measured for the brain tissues. Evidently, a trough of the absorbance spectra falls within window III, indicating the minimal absorbance in this window.

With the transmittance measured and by using the Beer-Lambert law Eq. (1), the attenuation length $l_{t_{obs}}$ was calculated as $l_{t_{obs}} = -z/\ln(T)$, where z is thickness of the tissue and "obs" stands for "observed experimentally". Figure 2a shows the spectra of $l_{t_{obs}}$ in brain tissues in the four optical windows, and Figure 2b summarizes the peak $l_{t_{obs}}$ of brain tissues in each optical window. Evidently, window III offers the maximal $l_{t_{obs}}$ for tissues with all thicknesses. Corresponding to these peak $l_{t_{obs}}$'s, the values of the observed attenuation coefficient $\mu_{t_{obs}}$ (= $1/l_{t_{obs}}$) are displayed in Table 2, where the minimal attenuations fall within window III. Here $l_{t_{obs}}$ and $\mu_{t_{obs}}$ are used instead of l_t and μ_t since $l_{t_{obs}}$ and $\mu_{t_{obs}}$ were obtained from experimental measurements and they are not equal to the theoretical l_t and μ_t (= $\mu_s + \mu_a$); instead, $\mu_{t_{obs}}$ is smaller than μ_t because in experiments the very forward directed scatter of tissue allowed some scatter photons to reach the narrow-solid-angle collector.

Light propagation through a tissue medium undergoes multiple scattering for NIR wavelengths. Multiple light scattering in medium splits the incident light into two components: a coherent (ballistic) and an incoherent (diffusive) component [3, 10]. The

Table 1 Peak transmittance T (%) of brain tissues measured in each optical window.

Window	Tissue thickness			
	50 µm	100 µm	150 µm	200 µm
I	77.3	59.8	43.0	37.4
II	81.5	67.5	54.5	50.4
III	82.9	70.5	58.1	54.6
IV	81.0	67.7	51.7	47.8

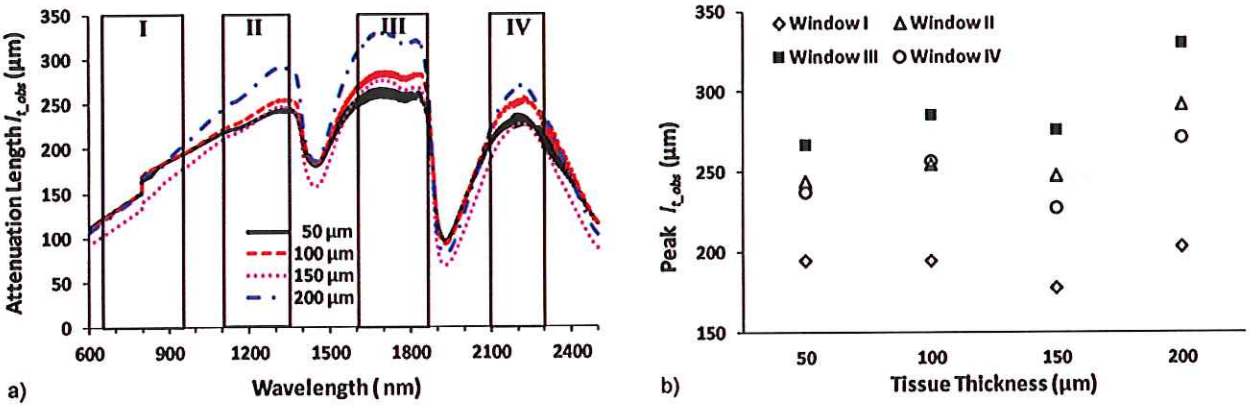

Figure 2 Spectra of the $l_{t_{obs}}$ (**a**) and peak $l_{t_{obs}}$ (**b**) in optical tissue windows I, II, III and IV. Brain tissue thicknesses were 50, 100, 150, and 200 μm respectively.

ballistic signal propagates undeviated in the forward direction and carries object information, while the diffusive light undergoes random walk in all directions and has more absorption than the ballistic light [11–13]. Incorporating the diffusive mode, Eq. (1) becomes [12, 14]

$$T = \frac{I}{I_0} = \exp\left(-\frac{z}{l_t}\right) + \frac{\Omega}{4\pi} \left[\sinh\left(\sqrt{\frac{3d^2}{l_{tr}l_a}}\left(1-\frac{z}{d}\right)\right)\right] \Big/ \left[2\sinh\left(\sqrt{\frac{3d^2}{l_{tr}l_a}}\right)\right], \quad (2)$$

where the first exponential term is the ballistic mode, and the second term is the diffusive mode; l_a is absorption length, and l_{tr} is transport length; Ω is the solid angle, for thin samples we use a small Ω, measured as ~10^{-2}; $d = z + 2z_0$, where $z_0 = 0.71l_{tr}$ [15]. Equation (2) can also be written as

$$T = \frac{I}{I_o} = \exp\left(-\frac{z}{l_t}\right) + \frac{\Omega}{4\pi}\exp\left(-\mu_{eff}z\right), \quad (3)$$

where

$$\mu_{eff} = \sqrt{3\mu_a(\mu_s' + \mu_a)}.$$

Table 2 Attenuation coefficient $\mu_{t_{obs}}$ (mm^{-1}) observed experimentally at corresponding peak attenuation lengths $l_{t_{obs}}$.

Window	Tissue thickness			
	50 μm	100 μm	150 μm	200 μm
I	5.14	5.14	5.63	4.92
II	4.10	3.93	4.04	3.43
III	3.75	3.50	3.62	3.03
IV	4.22	3.90	4.40	3.69

To evaluate the role that the ballistic and diffusive modes each plays in light transmission through thin brain tissues, simulations were performed using Eq. (3) for tissue thickness from 50 μm to 200 μm in the four optical windows and compared with experimental measurements of the peak transmittance. Model simulation results match well with the experiments in all four windows (Figure 3). The absorption coefficient μ_a chosen is in the range of 0.005–0.04 mm^{-1}. The reduced scattering coefficient μ_s' is between 0.5–10 mm^{-1} [16, 17]. In addition, μ_s' is known to decrease with wavelength and by using fitting equations and parameters of rat brain tissue given by Jacques [17], μ_s' was chosen within the range of 1–10 mm^{-1}, 0.2–4 mm^{-1}, 0.08–2 mm^{-1}, and 0.04–1 mm^{-1} for windows I, II, III, and IV, respectively. Table 3 shows the fitted values of l_t and reduced scattering coefficient μ_s' in each optical window, μ_a values were estimated from the absorption coefficient of water [18] by assuming water content of the brain is about 75% and therefore $\mu_a = 0.75\mu_{a_{water}}$, and corresponding values of g and μ_s that were calculated from these fitted parameters l_t, μ_a, and μ_s'. The value of g obtained from fitting slightly increases from 0.92 to 0.98 with the increase of wavelength because of the forward scattering generated by the large cell particles structure in tissue size from 2 μm to 20 μm, which is consistent with the study by Jacques (Figure 8) [17].

The column "exp avg. peak $l_{t_{obs}}$" in Table 3 is the average of the peak $l_{t_{obs}}$ for all tissues (thicknesses 50–200 μm) in that window, calculated from peak transmittance measured using Eq. (1) (Beer-Lambert law). Note that Eq. (1) only contains the ballistic mode of the light, and good agreements between $l_{t_{obs}}$ calculated using Eq. (1) and l_t fitted using Eq. (3) (ballistic and diffusive mode), these results suggest that in our experiments for brain tissue with thickness up to 200 μm, the ballistic mode plays a dominant role and the diffusive mode's role is trivial. As

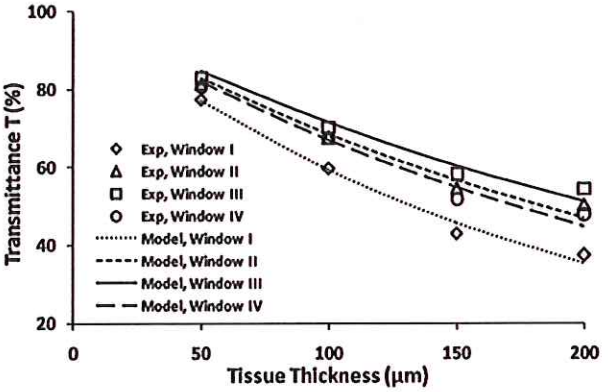

Figure 3 Comparison of peak transmittance from experiment and theoretical simulation for brain tissues in optical tissue windows I, II, III and IV.

the wavelength increases from window I to IV, the scattering coefficient decreases, allowing the absorption coefficient to have a slightly greater effect. It should be noted that this study more accurately obtained the attenuation length l_t (hence attenuation coefficient μ_t) in brain tissue, the values of g and μ_s were estimated after a certain range of μ_s' was chosen in each window.

The objective of this study was to find optimal optical windows for deep brain imaging. Present experiments on thin brain tissues have shown that window III is the best among four NIR windows for deep imaging in brain tissues. In addition, when using steady state absorption spectroscopy, the only way to estimate l_t from the ballistic part in tissue is to measure thin tissue samples, in which the ballistic part plays the dominant role; while the diffusive part cannot yield l_t directly if measuring thick tissue samples. Future studies may examine transmission in thicker brain tissue samples, which may more accurately specify optical parameters such as the reduced scattering coefficient μ_s', and compare with the present study on thin brain tissues slices.

In this study the optical parameters were investigated not only in windows II and III, but also in window IV which is centered at 2200 nm. These windows all show longer attenuation lengths than window I. However, not as presumed that window IV would be superior to window III, its attenuation length decreases from window III to the same level as window II. Other studies [19, 20] have also examined window III. Horton et al. [19] applied three photon microscopy for excitation of Texas red and red fluorescent protein at 1700 nm, but three photon fluorescence for excitation is not the optimal since the emission of such fluorophores is at ~585 nm and 613 nm respectively, which is not in any of the optical tissue windows. Deeper imaging may be achieved if both the excitation and emission wavelengths fall within the third optical window (1600 ~ 1870 nm). Therefore, the emission wavelength needs to be optimized into window III for deep brain imaging in future studies. Wang et al. [20] applied window III to pump and probe the overtones and combination modes of the methyl groups of proteins, amino acids, and lipids. Their studies showed that Window III gives greater penetration depth in tissue, which is consistent with the present study, but they did not look into the mechanisms of deep penetration in Window III, nor compared it with window IV.

In one study Sordillo et al. [6] reported the measurements of transmittance in four windows in the normal and cancerous prostate and breast tissues. Their study demonstrated the potential for deeper imaging, but no theoretical study was performed to explain their experimental observations. The present study further examined the transmission in brain tissue, and applied theoretical study to estimate optical parameters including l_t, μ_a and μ_s. In addition, the present study measured transmission in brain tissue, which contains more lipids than tissues measured in Sordillo's study. Both studies found window III is the optimal imaging window, suggesting that different lipid content in brain and other tissues may affect the absorption/scattering but did not make a difference in choosing the optimal window. Study by Caplan et al. [21] showed that the absorbance of cholesterol and cholesteryl oleate reached the maximum at ~1700 nm (window III) and the absorbance of collagen reached the highest and second highest in window IV and III respectively, which suggests window III an ideal window for examining cholesterol and collagen contents in different tissues. Future study on tissues from animals of the same species and ages are necessary for further validation and comparison between brain tissue and other tissues,

Table 3 Optical parameters for brain tissue in windows I, II, III, IV.

Window	Exp. avg. peak $l_{t_{obs}}$ (μm)	Model				
		l_t (μm)	μ_a (mm^{-1})	μ_s (mm^{-1})	g	μ_s' (mm^{-1})
I	192.4	191.2	0.0037	5.226	0.92	0.4
II	259.4	263.9	0.0743	3.715	0.95	0.2
III	289.7	296.4	0.5448	2.829	0.97	0.08
IV	248.1	248.7	1.4376	2.829	0.98	0.04

and for determining the effects of various tissue components, such as lipids, protein and collagen, in choosing the optimal windows.

The findings in this paper will be helpful for deep imaging of brain tissue in space and for increasing the imaging depth by using "gates" to select ballistic and snake photons. This information, in combination with new recent advances in brain network using one- and two-photon excitation in the NIR tissue windows II, III, and IV, will advance knowledge of the brain at the micrometer scale. The new CMOS cameras and photodetectors based on InSb for tissue imaging will improve imaging of brain blood vessels and extracellular space in vivo. Previous studies by Shi et al. [5] and Pu et al. [22] applied the technique of pumping fluorescent agent to its second excitation singlet (S_2) state to achieve greater imaging depth in rat brain tissue. The excitation and emission wavelengths both fall within the first optical window, whereas usually only one of the wavelengths is in the optical window (namely S_1 state). Deeper imaging in brain tissue may be achieved if applying this novel S_2 pumping technique while both excitation and emission wavelengths fall within window III, II, or IV.

4. Conclusion

In conclusion, the key optical lengths and attenuation coefficients for brain tissue in NIR windows were determined. The $l_{t_{obs}}$ was measured; μ_a, μ_s, g and μ_s' were estimated. It is evident that brain tissues become more transparent when using NIR optical windows centered at 1200 nm, 1700 nm, and 2200 nm due to reduction of multi-scattering at longer NIR wavelengths. Experiments on thin brain tissues suggested that among these four windows, covering from 1600 nm to 1870 nm is an optimal window for light penetration in brain tissue, and is followed by windows II and IV. Window III is called the Golden window.

Acknowledgements Thanks to Thomas Harvey and George Harvey for grammar checking of the manuscript. This work was supported by ARO (RRA) and NIH grants 5SC1HD068129 (ARC) and 2G12RR003060-26A1 from the National Center for Research Resources.

References

[1] H. McIlwain and H. S. Bachelard, Biochemistry and the central nervous system (Churchill Livingstone, Edinburgh; New York, 1985).
[2] L. Wang, P. P. Ho, C. Liu, G. Zhang, and R. R. Alfano, Science **253**, 769–771 (1991).
[3] R. R. Alfano, W. B. Wang, L. Wang, and S. K. Gayen, in PHOTONICS: Scientific Foundations, Technology and Applications, edited by D. L. Andrews (John Wiley & Sons, 2015).
[4] L. A. Sordillo, B. B. Das, Y. Pu, K. X. Liang, G. Milione, P. P. Sordillo, S. Achilefu, and R. R. Alfano, in Proc. SPIE, Vol. 8577, edited by R. R. Alfano and S. G. Demos (SPIE, 2013).
[5] L. Shi, A. Rodriguez-Contreras, Y. Budansky, Y. Pu, T. A. Nguyen, and R. R. Alfano, J. Biomed. Opt. **19**, 066009 (2014).
[6] L. A. Sordillo, Y. Pu, S. Pratavieira, Y. Budansky, and R. R. Alfano, J. Biomed. Opt. **19**, 056004 (2014).
[7] S. Adise, A. Saliu, N. Maldonado, V. Khatri, L. Cardoso, and A. Rodriguez-Contreras, J. Neurosci. **34**, 4528–4533 (2014).
[8] S. Miraux, J. M. Franconi, and E. Thiaudiere, Magn. Reson. Med. **56**, 469–473 (2006).
[9] A. K. Sinha, C. Cane, and S. T. Kempley, Arch. Dis. Child. Fet. Neonat. Ed. **91**, F31–F35 (2006).
[10] K. M. Yoo and R. R. Alfano, Opt. Lett. **15**, 320 (1990).
[11] K. M. Yoo, F. Liu, and R. R. Alfano, Phys. Rev. Lett. **64**, 2647–2650 (1990).
[12] K. M. Yoo, F. Liu, and R. R. Alfano, Opt. Lett. **16**, 1068–1070 (1991).
[13] G. E. Anderson, F. Liu, and R. R. Alfano, Opt. Lett. **19**, 981–983 (1994).
[14] M. Lax, V. Nayaranamurti, and R. C. Fulton, in Laser Optics of Condensed Matter, edited by J. Birman (Springer US, Plenum Press, New York, USA, 1988).
[15] R. Garg, R. K. Prud'homme, I. A. Aksay, F. Liu, and R. R. Alfano, J. Opt. Soc. Am. A. **15**, 932–935 (1998).
[16] D. T. Delpy and M. Cope, Philos. Trans. R. Soc. Lond. B. Biol. Sci. **352**, 649–659 (1997).
[17] S. L. Jacques, Phys. Med. Biol. **58**, R37–R61 (2013).
[18] G. M. Hale and M. R. Querry, Appl. Opt. **12**, 555–563 (1973).
[19] N. G. Horton, K. Wang, D. Kobat, C. G. Clark, F. W. Wise, C. B. Schaffer, and C. Xu, Nature Photon **7**, 205–209 (2013).
[20] P. Wang, H. W. Wang, M. Sturek, and J. X. Cheng, J. Biophotonics **5**, 25–32 (2012).
[21] J. D. Caplan, S. Waxman, R. W. Nesto, and J. E. Muller, J. Am. Coll. Cardiol. **47**, C92–C96 (2006).
[22] Y. Pu, L. Shi, S. Pratavieira, and R. R. Alfano, J. Appl. Phys. **114**, 153102 (2013).